Mass spectra and theoretical modeling of Li^+Ne_n, Li^+Ar_n and Li^+Kr_n clusters

George E. Froudakis [a,b], Stavros C. Farantos [a,b], Michalis Velegrakis [a,*]

[a] *Institute of Electronic Structure and Laser, Foundation for Research and Technology-Hellas, P.O. Box 1527, 711 10 Heraklion, Crete, Greece*

[b] *Department of Chemistry, University of Crete, 711 10 Heraklion, Crete, Greece*

Received 27 March 2000

Abstract

The mass spectra of the Li^+X_n (X = Ne, Ar, Kr) clusters have been recorded with a time-of-flight apparatus. In the mass spectra, the peaks that correspond to Li^+X_4 and Li^+X_6 indicate very stable clusters. Relatively high intensity, with respect to neighboring ones, is also observed for the clusters with 34 argon or krypton atoms. To unravel the geometries of these species, we perform Møller–Plesset perturbation theory of second order for the small size Li^+Ne_n and Li^+Ar_n clusters and molecular dynamics quenching minimization calculations for the larger Li^+Ar_n complexes. Regular octahedral geometries are found for Li^+X_6, whereas for Li^+Ar_{34} a closed packed geometry with an octahedral core is identified as the lowest minimum energy structure. The latter is further supported by MP2 calculations. © 2000 Elsevier Science B.V. All rights reserved.

1. Introduction

Aggregation of atoms and molecules with weak interactions such as van der Waals forces have been studied for several years. Their interest stems in understanding the properties of the system from small size clusters to macroscopic states. However, it was soon discovered that clusters might have their own importance since they present properties, which are not encountered either in the monomers or in the macroscopic states. Small size clusters allow accurate theoretical calculations and detailed experimental observations. This close co-operation between theory and experiment can result in a detailed description of the species.

In the last years, we have pursued such an experimental–theoretical project which involves the study of metal ion-doped noble gas clusters of the type MX_n (M = metal ion and X = noble gas atom). These clusters constitute prototype systems in modeling metal–ligand interactions, ranging from the gas phase diatomic complexes up to the bulk phase. Therefore, studies on these systems have been evolved in the last years in this topic of considerable interest [1–3].

Among the doped noble gas cluster systems studied by us are alkaline earth (Mg, Sr) [4–8], alkaline (K, Na) [6,9], group III (In, Al) [9], carbon [10,11] and transition metals (Ti, Fe, Ni, Pt) [12–14]. Clusters involving alkali metal ions, such as sodium and potassium, were among the first,

---

* Corresponding author. Tel.: +30-81-391-122; fax: +30-81-391-318.

E-mail address: vele@iesl.forth.gr (M. Velegrakis).

which were studied because of the simple electronic configuration of the metal [15,16]. If the metal exhibits a s orbital or any spherical electronic configuration the noble gas atoms tend to arrange around the central metal core and the cluster structure is then dictated by geometrical factors, such as the atomic size ratio. Such arrangements have often been observed in the mass spectra of MX_n cluster systems [4,5] and have also been successfully explained [6,8]. However, the detailed balance of the attractive and repulsive forces in the cluster may result in stable structures with the metal cation on the surface. This was found in Mg^+Ar_{12} complex [7].

Clusters of Li^+ with one and two noble gas atoms were studied by Bauschlicher and coworkers [17–19] with ab initio methods, and the results were favorably compared with the experiment. Configuration interaction (CI) calculations have also been performed by Iwata and co-workers for the diatomics Li^+Ne and Li^+Ar [20,21] in order to simulate their ultraviolet emission spectra. Surprisingly, to the best of our knowledge there are no studies of Li^+X_n with a large number of rare gas. The purpose of the present article is to investigate large inert gas clusters of lithium cation. We present mass spectra for Li^+Ne_n, Li^+Ar_n and Li^+Kr_n clusters which show that lithium can be bounded with tens of inert gas atoms. The accompanied theoretical first principle calculations are mainly restricted to small size clusters, but they are sufficient to explain the first magic numbers and the nature of forces exerted from Li^+ to Ne and Ar atoms. Additionally, molecular dynamics simulations with quenching minimization techniques have been performed in order to determine the geometries of larger clusters and in particular for Li^+Ar_{14} and Li^+Ar_{34} which show an enhanced stability in the mass spectra. Li^+Ar_{34} shows the interesting structure of a closed packed geometry with an octahedral core. This is supported by MP2 calculations.

2. Experimental methods

The experimental setup used for the production of Li^+X_n complexes and the time-of-flight (TOF)

apparatus are the same used in our previous studies [5,10]. For completeness of the paper we give a brief description in the following.

The molecular beam apparatus consists of three differentially pumped chambers, and it is equipped with a TOF mass spectrometer. The Li^+-doped rare gas clusters are formed in a laser vaporization source, where a pulsed infrared Nd:YAG laser produces plasma from a pure Li target. The plasma plume is mixed with an expanding gas pulse provided by a home built nozzle. The adiabatic expansion results in cooling of the nascent clusters, thus forming a cluster beam which contains neutral clusters as well as ionic species. We study the positive ions, which are produced directly from the plasma/noble gas mixing without the use of post-ionization. Hence, it is expected that these clusters are sufficiently relaxed and the measured size distribution reflects the stability of these species.

The cluster ions produced enters via a skimmer in the acceleration chamber where a pulsed double field acceleration unit directs the ions through a collimator towards the third chamber that houses the detection assembly for the TOF analysis of the produced ions. The ions are measured with two microchannel plate (MCP) detectors using two different operation modes, the linear and the reflecting. In the first case, a MCP can be inserted externally (through a vacuum translator) perpendicular to the spectrometer axis, while in the latter case a second MCP is placed off-axis in order to measure the backwards reflected ions from a reflectron assembly. In both cases, the MCP output is directly connected to a computer controlled digital storage oscilloscope, where the TOF mass spectra are acquired and stored shot by shot. The spectra that will be discussed are obtained by averaging several hundreds of single shot spectra.

3. Theoretical methods

The theoretical treatment of Li ion-doped neon and argon aggregates involved the Møller–Plesset perturbation theory of second order (MP2) [22]. The atomic basis set that we use includes Gaussian functions of triple zeta quality augmented by d-polarization functions (6-311G*) [23]. In order to

check the accuracy of the calculations at the MP2/6-311G* level, we also performed calculations either with methods treating better the electron correlation like coupled-clusters with single and double and a perturbative estimation of the triple excitations (CCSD(T)), or using larger and more accurate basis sets like the correlation consistent (CC) basis set of Dunning and coworkers (doubly augmented double zeta for Ar) [24]. In both tests, the results were in satisfactory agreement with the MP2/6-311G* as is shown in Section 4. All the geometries found here are fully optimized with the method mentioned above. The calculations were performed with the GAUSSIAN 94 package of programs [23]. For large clusters, the method of molecular dynamics accompanied by quenching the energy of the cluster is used to locate minimum energy structures [6]. More details are given in Section 4.

4. Results and discussion

In Fig. 1, we show the TOF spectra of $Li^+–Ne_n$, $Li^+–Ar_n$ and $Li^+–Kr_n$. Depending on the intensity of the produced ions, the spectra are obtained either with the linear or the reflecting setup. Therefore, the TOF scale differs for some systems. For Li^+Ar_n and Li^+Kr_n, clusters with more than 200 atoms are recorded. In the spectra of Fig. 1, the most stable clusters are labeled with the number n of the noble gas atoms. Stable clusters are defined as those clusters whose corresponding peaks exhibit an enhanced intensity in the recorded mass spectra. We characterize a particular cluster as specially stable by using two criteria. (i) The peak that corresponds to the particular cluster size must differ at least 10% from the neighboring ones, and (ii) this behavior has to be independent of the source conditions (inlet pressure, laser fluence, ablation point distance from the nozzle, etc.).

The common feature in the mass spectra of Fig. 1 is the extra stability appearing for clusters with $n = 4$ and 6 noble gas atoms. The variations in the intensities of Li^+Ne_n and for $n = 2–6$ are small compared to those of argon and krypton. Furthermore, for the cases of argon and krypton, a pronounced peak appears at $n = 34$, indicating a
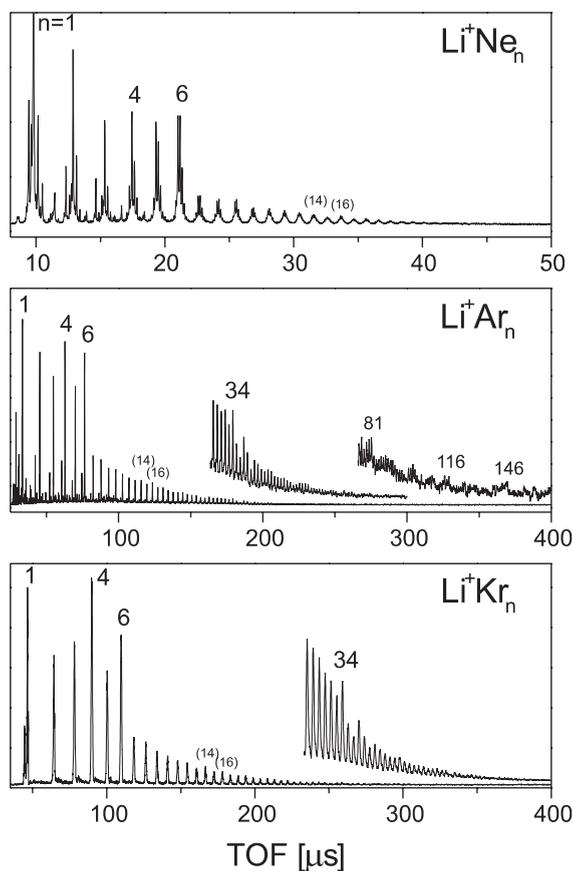

Fig. 1. TOF spectra of Li^+Ne_n, Li^+Ar_n and Li^+Kr_n clusters. The most stable clusters are indicated with the number n of noble gas atoms. Labels in parentheses denote less pronounced clusters.

special stability for the complex Li^+X_{34}. Less pronounced, but always reproducible peaks appear at $n = 14$ and 16 for all systems in Fig. 1.

4.1. Ab initio calculations

We seek the minimum energy structures of Li^+Ne_n and Li^+Ar_n ($n = 1–7$) clusters by performing first principle optimization calculations. Various initial geometries were tested for each cluster at the MP2/6-311G* level of theory in order to obtain the absolute minimum. The total energy, E_{tot}, the binding energies, $E(n) = E_{tot} - E(Li^+) - nE(X)$, of these minima and the charge on Li (obtained from a Mulliken population analysis)

Table 1
Total and binding energies of Li^+Ne_n and Li^+Ar_n ($n = 1$–7) clusters obtained at the MP2/6-311G* level of theory[a]

n	Li^+Ne_n			Li^+Ar_n		
	Total energy (Hartree)	Binding energy (eV)	Charge on Li	Total energy (Hartree)	Binding energy (eV)	Charge on Li
0	−7.235840		1.00	−7.235840		1.00
1	−135.983399	0.23	0.96	−534.201992	0.29	0.87
2	−264.731192	0.46	0.92	−1061.169047	0.61	0.72
3	−393.478679	0.69	0.88	−1588.132906	0.85	0.64
4	−522.226089	0.91	0.86	−2115.096506	1.07	0.56
5	−650.972492	1.10	0.84	−2642.055279	1.17	0.53
6	−779.719009	1.30	0.82	−3169.015846	1.31	0.46
7	−908.460254	1.35	0.81	−3695.971797	1.33	0.46

[a] The charge on the Li atom is that of Mulliken population analysis.

are listed in Table 1. Their geometrical parameters are presented in Table 2.

The ground electronic state of Li^+Ne is a $^1\Sigma^+$ state with a bond length of 2.050 Å and binding energy of 0.23 eV, while for Li^+Ar our calculations show a state of the same symmetry with a bond distance of 2.347 Å and binding energy of 0.29 eV. More accurate, CCSD(T)/6-311G*, calculations for Li^+Ar give a bond distance of 2.343 Å and binding energy of 0.30 eV, which are in accord to the MP2 results. Comparing with the results of Bauschlicher et al. [19] who carried out MCPF calculations and found a bond length for Li^+Ar of

2.423 Å and binding energy 0.238 eV we can see that the MP2 results predict a shorter bond length and an increased dissociation energy. For the same system, the CI calculations by Iwata and co-workers [20,21] gave a bond distance of 2.48 Å and binding energy 0.297 eV. For Li^+Ne, the same investigators obtained an equilibrium bond distance of 2.00 Å and dissociation energy 0.161 eV.

For both Li^+Ne_2 and Li^+Ar_2, a linear geometry is predicted with a $^1\Sigma_g^+$ ground state. The equilibrium bond distances are 2.043 and 2.324 Å, respectively, and the binding energies are 0.46 and 0.61 eV as can be seen in Tables 1 and 2. Any

Table 2
Structural characteristics of Li^+Ne_n and Li^+Ar_n ($n = 1$–7) clusters obtained at the MP2/6-311G* level of theory[a]

System	Symmetry	Structural characteristics	
Li^+Ne	$C_{\infty v}$	Li–Ne = 2.050	
Li^+Ne_2	$D_{\infty h}$	Li–Ne = 2.043	
Li^+Ne_3	C_{2v}	Li–Ne$_{top}$ = 2.053	Li–Ne$_{bot}$ = 2.045
		Ne$_{top}$–Li–Ne$_{bot}$ = 109°	Ne$_{top}$–Ne$_{bot}$ = 3.340
Li^+Ne_4	T_d	Li–Ne = 2.050	Ne–Ne = 3.348
Li^+Ne_5	C_{4v}	Li–Ne$_{top}$ = 2.082	Li–Ne$_{base}$ = 2.097
		Ne$_{top}$–Ne$_{base}$ = 3.164	Ne$_{base}$–Ne$_{base}$ = 2.934
Li^+Ne_6	O_h	Li–Ne = 2.119	Ne–Ne = 2.995
Li^+Ne_7	C_s	Ne–Ne$_{oct}$ = 2.774	
Li^+Ar	$C_{\infty v}$	Li–Ar = 2.347	
Li^+Ar_2	$D_{\infty h}$	Li–Ar = 2.324	
Li^+Ar_3	D_{3h}	Li–Ar = 2.353	Ar–Ar = 4.076
Li^+Ar_4	T_d	Li–Ar = 2.390	Ar–Ar = 3.903
Li^+Ar_5	C_{4v}	Li–Ar$_{top}$ = 2.462	Li–Ar$_{base}$ = 2.499
		Ar$_{top}$–Ar$_{base}$ = 3.738	Ar$_{base}$–Ar$_{base}$ = 3.502
Li^+Ar_6	O_h	Li–Ar = 2.539	Ar–Ar = 3.591
Li^+Ar_7	C_s	Ar–Ar$_{oct}$ = 4.071	

[a] Bond lengths are in Å and bond angles in degrees.

attempt starting from a bent triangular geometry, after the geometry optimization ends up in the linear configuration, indicating that there is no bent local minimum. These results were tested with CCSD(T) calculations and CC basis sets which treat the electron correlation more accurate. Our calculations on Li^+Ar_2 can also be compared with those of Bauschlicher et al. [19] who found a bond length of 2.428 Å and binding energy of 0.510 eV.

In Li^+Ne_3 and Li^+Ar_3 clusters, the ground state geometries are of different symmetry. Li^+Ne_3 is a planar C_{2v} structure with the Li ion in the middle connected with the three Ne atoms. The Li–Ne bonds are one 2.053 Å and two 2.045 Å, while the two Ne–Ne bonds are 3.340 Å. On the other hand, the Li^+Ar_3 ground state geometry is a D_{3h} structure with the Li ion in the center. The Li–Ar bonds are 2.353 Å and the Ar–Ar bonds are 4.076 Å. It is argued that the lower symmetry found for Li^+Ne_3 is due to the shorter Li^+–Ne interactions which make the two Ne atoms to approach each other, thus, increasing the repulsion. The binding energies of Li^+Ne_3 and Li^+Ar_3 are 0.69 and 0.85 eV, respectively. It is worth reporting that all pyramidal or planar initial geometries, after the geometry optimization end up into C_{2v} and D_{3h} geometries for Li^+Ne_3 and Li^+Ar_3, respectively.

Li^+Ne_4 and Li^+Ar_4 were found to have a tetrahedral geometry with the Li ion in the center. The geometrical parameters are given in Table 2. The binding energies are 0.91 eV for Li^+Ne_4 and 1.07 eV for Li^+Ar_4. For both systems, a local minimum with a square geometry was located. In Li^+Ar_4, this square configuration lies 2.3 kcal/mol above the absolute minimum, while in Li^+Ne_4 the energy difference is 0.5 kcal/mol.

For Li^+Ne_5 and Li^+Ar_5, two structures are competing for the ground state of the complex: the square pyramid and the triangular bipyramid. In both systems, the first is lower in energy by 0.1 kcal/mol in Li^+Ne_5 and 0.3 kcal/mol in Li^+Ar_5. With the present accuracy of our calculations, it is difficult to unequivocally characterize the absolute minimum. An attempt to separate energetically these two structures in Li^+Ar_5 with a larger and more accurate basis set (CC) ends up to the same conclusion as with the 6-311G* basis set and to the same energy difference (0.27 eV).

In Li^+Ne_5, the square pyramid has a binding energy of 1.10 eV and the Li ion lies in the center and 10° above the plane of neon atoms. The Li–Ne_{top} distance is 2.082 Å, the Li–Ne_{base} is 2.097 Å, the Ne_{top}–Ne_{base} is 3.164 Å and the Ne_{base}–Ne_{base} is 2.934 Å. The triangular bipyramid has two Li–Ne bonds of 2.106 Å, three of 2.085 Å, three Ne–Ne bonds of 3.612 Å and six Ne–Ne bonds of 2.964 Å. The binding energy of Li^+Ar_5 is 1.17 eV for the square pyramid. As in the case of neon, the Li ion lies 10° above the plane of four argon atoms.

Li^+Ne_6 and Li^+Ar_6 have an octahedral geometry at the lowest energy with the Li ion in the center. The binding energies are 1.30 and 1.31 eV for neon and argon, respectively. In both systems, no other local minima were found. The geometrical parameters are tabulated in Table 2.

For clusters with more than six ligands, the extra atoms are capping the faces of the octahedron. Li^+Ne_7 and Li^+Ar_7 have binding energy of 1.35 and 1.33 eV, respectively, while the Ne–Ne bonds are 2.774 Å and the Ar–Ar bonds 4.071 Å. Thus, we find that the binding energy for neon clusters is now larger than that of argon complexes. An explanation can be given by taking into account the small size of neon atom, which makes the electrostatic attractive forces to dominate with respect to the repulsion of electrons. This results in a deformation of the octahedron of lithium–neon complex, thus, allowing all Ne atoms to be as close to the positive charge as possible. Contrary to that, in the argon clusters the octahedron is only slightly deformed.

The energy differences of the clusters, $E(n)-E(n-1)$, are plotted in Fig. 2. Assuming that such energy differences reflect the stability of the complex with respect to neighboring ones, the comparison of these plots with the mass spectra in Fig. 1 is rather satisfactory. Particularly, the closed shell structures for $n = 6$ can explain the abrupt decrease in the binding energies of the larger clusters.

Furthermore, we observe that for Li^+Ne_n, $n = 1–6$, the interaction energies are almost pair additive, in contrast to argon clusters for which we find fluctuations in the binding energies. This is attributed to the higher polarizability of Ar. The induced dipoles and the resulting interactions of
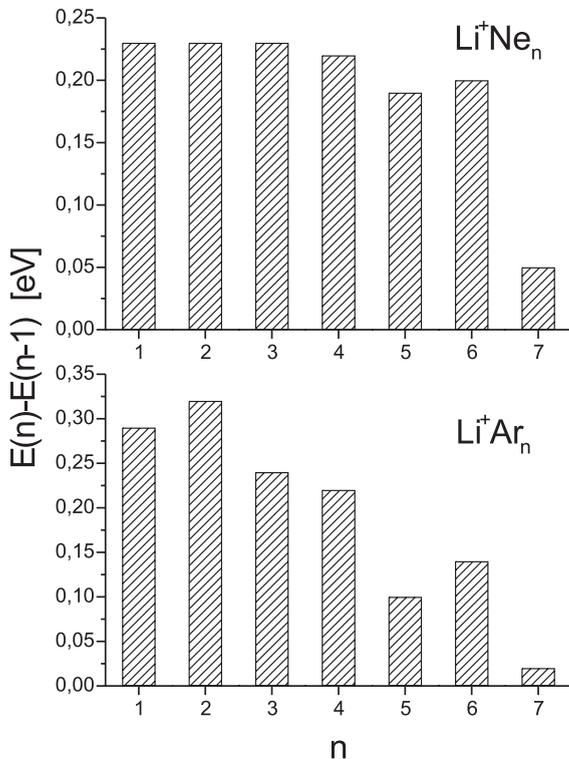
Fig. 2. Energy differences, $E(n) - E(n-1)$, as a function of number n of rare gas atoms in the clusters.

charge-induced dipoles and induced dipole–induced dipole among argon atoms [7] make the many body terms in the potential to be more important for argon than for neon.

4.2. Molecular dynamics simulations

The above ab initio calculations have shown that for all cluster systems there is a first shell closure that occurs at $n = 6$ resulting in an octahedral Li^+X_6 cluster. A pure geometrical scenario for the cluster growth would require 19 noble gas atoms to form a perfect octahedral second shell Li^+X_{19} cluster [25]. From the TOF spectra however we do not observe any irregularity at $n = 19$. Instead, the mass spectrum reveals that a relatively stable complex is formed at $n = 14$ and for the systems Li^+Ar_n and Li^+Kr_n the intensity for the clusters Li^+Ar_{34} and Li^+Kr_{34} is very pronounced (Fig. 1).

In order to determine the structural trends in the Li^+X_n clusters, we have performed molecular dynamics calculations for $n = 14$ and $n = 34$ for the argon complexes. Specifically, we have studied the Li^+Ar_6, Li^+Ar_{14}, and Li^+Ar_{34} clusters. We use pair additive Lennard-Jonnes potentials for Li^+–Ar and Ar–Ar interactions. In this manner, we employ the procedure presented in our previous paper [6], i.e., we use reduced units for energies ε^* and distances σ^*, where $\varepsilon^* = \varepsilon^+_{Li-Ar}/\varepsilon_{Ar-Ar} \approx 25$ and $\sigma^* = \sigma^+_{Li-Ar}/\sigma_{Ar-Ar} \approx 0.65$, ($\varepsilon_{Ar-Ar} = 12.5$ meV and $\sigma_{Ar-Ar} = 3.3$ Å). Minimization of the potential energy with the quenching method gives the lowest minimum energy configurations shown in Fig. 3.

We first carry out calculations for Li^+Ar_6 in order to compare the minimum energy geometry with that obtained from the ab initio calculations. Indeed, a minimum octahedral (OCT) structure is found in agreement with the ab initio results. The structure labeled ICO in Fig. 3 is a pentagonal bipyramid and constitutes the basis of the growth of the icosahedral clusters as was found in Mg^+Ar_n [6,7] and K^+Ar_n [6]. It lies higher in energy than the octahedral geometry.

For Li^+Ar_{14} the asymmetric structure which has the Ar atoms in one side of the octahedron is lower than the symmetric face centered cubic (FCC) ge-
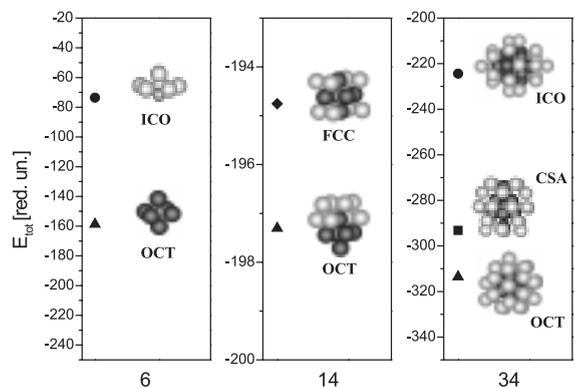

Fig. 3. Minimum energy geometries of Li^+Ar_n clusters and for $n = 6$, 14 and 34. OCT refers to an OCT geometry core in the cluster; ICO, an icosahedral; FCC, a face centered cubic and CSA, a capped square antiprism core. The structures were obtained by molecular dynamics minimization techniques (see text).

ometry (Fig. 3). This is because the former structure maximizes the number of Ar–Ar interactions.

The case of Li^+Ar_{34} is of special interest. Here the structure labeled OCT is the absolute minimum as is evident by comparing the ICO conformation and a structure based on a capped square antiprism (CSA) (Fig. 3). The OCT structure constitutes in fact a close packed cluster with an OCT core. This results in a very dense packing around a perfect octahedron. To the best of our knowledge, such a dense structure containing a perfect OCT core has not been reported before. To further illustrate the geometry of Li^+Ar_{34} cluster in Fig. 4, we built up this structure in three steps by starting from the octahedron. By adding four atoms at the triangular faces a perfect tetrahedron with $n = 10$ atoms is obtained. Placing three argon atoms at each side of the tetrahedron (another 12 Ar atoms), we construct the geometry shown in Fig. 4 with $n = 22$. Finally, the Li^+Ar_{34} is formed by adding another 12 atoms (two atoms in each of the six vertices of the $n = 10$ tetrahedron). It should be emphasized that the intermediate geometries shown in Fig. 4 are not stable structures.

In order to solidify the above results of Li^+Ar_{34}, we have carried out a series of calculations for this species at the MP2 level of theory. With the current computer facilities available to us it was possible to use the double zeta basis set 6-31G*. Our strategy was the following. The location of the minimum was done at the Hartree–Fock (HF) level using the basis set 3-21G* and keeping the initial symmetry of the cluster constant. The symmetry for the three isomers are T_d for the OCT, D_{4d} for the CSA and D_{5d} for the ICO complex. After the HF geometry optimization, a single point MP2/6-31G* calculation is done at the located minimum to compute the energy.

In both theoretical levels (HF/3-21G* and MP2/6-31G*), the OCT geometry is the lowest in energy confirming the molecular dynamics results. The energy differences among the structures CSA–OCT and ICO–OCT are 0.17 and 0.33 eV, respectively, at the HF level and 0.31 and 0.51 eV at the MP2 level. The harmonic frequency analysis which was done at the HF level of theory predict a true minimum for the lowest octahedral geometry but imaginary frequencies for the other two
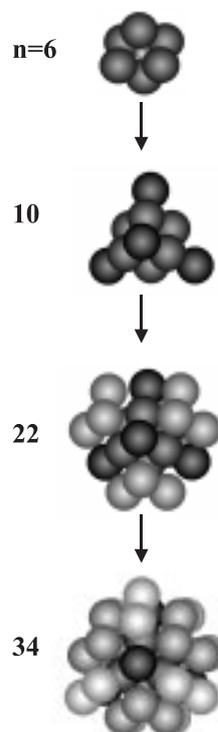

Fig. 4. Building the Li^+Ar_{34} cluster in three steps starting with an OCT Li^+Ar_6 core.

structures. This indicates that these structures (CSA and ICO) constitute saddle points in the multidimensional potential energy surface.

Considering now the stability and the structural properties of alkali ion-doped argon clusters we establish that the size of the ion plays a major role in the growth sequences and in the geometrical structures of these clusters. Among the different alkali ions the atomic size ratio σ^* varies from 0.84 for K^+–Ar [6] to 0.75 for Na^+–Ar [9] to 0.65 for Li^+–Ar. The structures observed in the mass spectra of these systems are based on icosahedron for K^+–Ar_n [6], on capped square antiprism for Na^+–Ar_n [9] and on octahedron for Li^+–Ar_n. This is in excellent agreement with the predictions of the simple hard sphere packing model of Refs. [6,9], where for $0.95 \geqslant \sigma^* > 0.822$ the geometry of the clusters is based on an icosahedral (ICO) core, for $0.822 \geqslant \sigma^* > 0.707$ on a capped square antiprism and for $0.707 \geqslant \sigma^* > 0.6125$ on an octahedral core. A thorough review concerning atomic

size effects in the stability, structure and optical properties of ion-doped noble gas clusters can be found in Ref. [26].

5. Conclusions

To summarize, from the experimental–theoretical study of the structures of Li^+X_n, we conclude that the first closed shell geometries are octahedral. In the case of Li^+Ar_n and Li^+Kr_n, large clusters are formed. Thus, it was possible to show that 34 argon atoms are needed to fill the second shell (Fig. 4). One important outcome of the present work is the reversion observed in the binding energies of Li^+Ne_n and Li^+Ar_n with $n = 7$. In other words, the inert gas atoms are bounded tighter in the neon cluster than in argon something which is not expected for the small complexes.

References

[1] D.E. Lessen, R.L. Asher, P.J. Brucat, in: M.A. Duncan (Ed.), Advances in Metal and Semiconductor Clusters, vol. I, JAI Press, Greenwich, 1993.

[2] C.W. Bauschlicher Jr., Partridge, H. Langhoff, S.R. in: M.A. Duncan (Ed.), Advances in Metal and Semiconductor Clusters, vol. II, JAI Press, Greenwich, 1994.

[3] W.H. Breckenridge, C. Jouvet, B. Soep, in: M.A. Duncan (Ed.), Advances in Metal and Semiconductor Clusters, vol. III, JAI Press, Greenwich, 1995.

[4] M. Velegrakis, Ch. Lüder, Chem. Phys. Lett. 223 (1994) 139.

[5] Ch. Lüder, M. Velegrakis, J. Chem. Phys. 105 (1996) 2167.

[6] D. Prekas, Ch. Lüder, M. Velegrakis, J. Chem. Phys. 108 (1998) 4450.

[7] G.S. Fanourgakis, S.C. Farantos, J. Phys. Chem. 100 (1996) 3900.

[8] G.S. Fanourgakis, S.C. Farantos, Ch. Lüder, M. Velegrakis, S.S. Xantheas, J. Chem. Phys. 109 (1996) 108.

[9] Ch. Lüder, D. Prekas, M. Velegrakis, Laser Chem. 17 (1997) 109.

[10] Ch. Lüder, E. Georgiou, M. Velegrakis, Int. J. Mass Spectrom. Ion Process. 153 (1996) 129.

[11] G.E. Froudakis, G.S. Fanourgakis, S.C. Farantos, S.S. Xantheas, Chem. Phys. Lett. 294 (1998) 109.

[12] M. Velegrakis, G.E. Froudakis, S.C. Farantos, Chem. Phys. Lett. 302 (1999) 595.

[13] S. Bililign, C.S. Feigerle, J.C. Miller, M. Velegrakis, J. Chem. Phys. 108 (1998) 6312.

[14] M. Velegrakis, G.E. Froudakis, S.C. Farantos, J. Chem. Phys. 109 (1998) 4687.

[15] P. Ru-Pin, R.D. Etters, J. Chem. Phys. 72 (1980) 1741.

[16] G.R. Ahmadi, J. Almlof, I. Roeggen, Chem. Phys. 199 (1996) 33.

[17] H. Partridge, C.W. Bauschlicher Jr., S.R. Langhoff, J. Phys. Chem. 96 (1992) 5350.

[18] H. Partridge, C.W. Bauschlicher Jr., J. Phys. Chem. 98 (1994) 2301.

[19] C.W. Bauschlicher Jr., H. Partridge, S.R. Langhoff, Chem. Phys. Lett. 165 (1990) 272.

[20] S. Iwata, S. Nanbu, H. Kitajima, J. Chem. Phys. 94 (1991) 3707.

[21] M. Hiyama, S. Nanbu, S. Iwata, Chem. Phys. Lett. 192 (1992) 443.

[22] A. Szabo, N.S. Ostlund, Modern Quantum Chemistry: Introduction to Advanced Electronic Structure Theory, Dover, NY, 1989.

[23] M.J. Frisch, G.W. Trucks, H.B. Schlegel, P.M.W. Gill, B.G. Johnson, M.A. Robb, J.R. Cheeseman, T. Keith, G.A. Petersson, J.A. Montgomery, K. Raghavachari, M.A. Al-Laham, V.G. Zakrzewski, J.V. Ortiz, J.B. Foresman, J. Cioslowski, B.B. Stefanov, A. Nanayakkara, M. Challacombe, C.Y. Peng, P.Y. Ayala, W. Chen, M.W. Wong, J.L. Andres, E.S. Replogle, R. Gomperts, R.L. Martin, D.J. Fox, J.S. Binkley, D.J. Defrees, J. Baker, J.P. Stewart, M. Head-Gordon, C. Gonzalez, J.A. Pople, GAUSSIAN 94, Revision D.4, Gaussian Inc., Pittsburgh, PA, 1995.

[24] D.E. Woon, J.T.H. Dunning, J. Chem. Phys. 100 (1994) 2975.

[25] T.P. Martin, T. Bergmann, H. Gohlich, T. Lange, J. Phys. Chem. 95 (1991) 6421.

[26] M. Velegrakis , in: M.A. Duncan (Ed.), Advances in Metal and Semiconductor Clusters, vol. V, JAI Press, Greenwich, in press.